# Theory of graphene saturable absorption

A. Marini,[1,*] J. D. Cox,[1] and F. J. García de Abajo[1,2]

[1]*ICFO-Institut de Ciencies Fotoniques, The Barcelona Institute of Science and Technology, 08860 Castelldefels (Barcelona), Spain*

[2]*ICREA-Institució Catalana de Recerca i Estudis Avançats, Passeig Lluís Companys 23, 08010 Barcelona, Spain*

(Received 9 May 2016; revised manuscript received 13 January 2017; published 6 March 2017)

Saturable absorption is a nonperturbative nonlinear optical phenomenon that plays a pivotal role in the generation of ultrafast light pulses. Here we show that this effect emerges in graphene at unprecedentedly low light intensities, thus opening avenues to new nonlinear physics and applications in optical technology. Specifically, we theoretically investigate saturable absorption in extended graphene by developing a semianalytical nonperturbative single-particle approach, describing electron dynamics in the atomically-thin material using the two-dimensional Dirac equation for massless Dirac fermions, which is recast in the form of generalized Bloch equations. By solving the electron dynamics nonperturbatively, we account for both interband and intraband contributions to the intensity-dependent saturated conductivity and conclude that the former dominates regardless of the intrinsic doping state of the material. We obtain results in qualitative agreement with atomistic quantum-mechanical simulations of graphene nanoribbons including electron-electron interactions, finite-size, and higher-band effects. Remarkably, such effects are found to affect mainly the linear absorption, while the predicted saturation intensities are in good quantitative agreement in the limit of extended graphene. Additionally, we find that the modulation depth of saturable absorption in graphene can be electrically manipulated through an externally applied gate voltage. Our results are relevant for the development of graphene-based optoelectronic devices, as well as for applications in mode-locking and random lasers.

DOI: 10.1103/PhysRevB.95.125408

## I. INTRODUCTION

Saturable absorption (SA) is an extreme nonlinear phenomenon that consists of the quenching of optical absorption under high-intensity illumination. This effect, which is an inherent property of photonic materials, constitutes a key element for passive mode-locking (PML) in laser cavities [1,2], where continuous waves are broken into a train of ultrashort optical pulses. Most materials undergo saturable absorption at very high optical intensities, in close proximity to their optical damage threshold. Currently, state-of-the-art semiconductor-based SA mirrors are routinely employed for PML lasers [3–5]. However, these mirrors operate in a narrow spectral range, are poorly tunable, and require advanced fabrication techniques.

Recently, carbon nanomaterials have emerged as an attractive, viable, and cost-effective alternative for the development of next-generation PML lasers. For example, carbon nanotubes (CNTs) undergo SA at rather modest light intensities, while their operation wavelength (determined by the energy band gap) can be manipulated by tuning their diameter [6–10]. Broadband operation has been demonstrated by using an ensemble of CNTs with a wide distribution in diameter, at the expense of higher linear loss from off-resonance tubes [8]. Graphene overcomes this limitation thanks to its peculiar conical band structure, which gives rise to broadband resonant SA at remarkably low light intensity [10–18] that can further be tuned by means of an externally applied gate voltage [19]. Graphene-based SA components have been used to achieve PML ultrafast laser operation [20,21], broadband tunability [22], and quality-factor switching [23]. Graphene multilayers have also been employed to generate large energy pulses [24] and to achieve PML in fiber lasers with normal dispersion [25]. In addition, recent theoretical investigations predict single-mode operation of random lasers by embedding graphene flakes in a gain medium [26].

Stimulated by the rising interest in SA of graphene for developing the above mentioned applications, several theoretical approaches have been proposed over the last few years to describe and understand this phenomenon. Pioneering efforts [27–29] accounting only for intraband electronic transitions in graphene predict high nonlinearities associated with harmonic generation, but graphene SA necessitates a more rigorous theoretical treatment, as it mainly arises from the interplay of intraband and interband dynamics: While the purely-intraband nonlinear response of graphene can be described semianalytically [27–29], interband processes are more complex. Subsequent semianalytical approaches accounting for combined interband and intraband processes have relied on perturbative expansions, which yield nonlinear conductivities for graphene [30–36] that accurately predict the SA threshold only when graphene is doped. In fact, such nonlinear conductivities are ill-defined for undoped graphene and diverge due to the Dirac point singularity, emphasizing the highly nonperturbative behavior of electrons in the carbon monolayer. Further investigations have resorted to computationally-demanding numerical time-domain integration of the graphene Bloch equations [17,37,38], which unfortunately provides little physical insight into electron dynamics. Despite the rapidly-growing body of research on graphene nonlinear optics, an accurate and transparent nonperturbative and semianalytical theory accounting for both intraband and interband dynamics is still missing. The single-particle massless Dirac fermion (MDF) picture [39] appears to be an appropriate theoretical framework for achieving this objective.

In this paper, we calculate intraband and interband contributions to SA of extended graphene by nonperturbatively

*andrea.marini@icfo.es

 

and semianalytically solving the single-particle Dirac equation for MDFs in the presence of an external electromagnetic field retaining only one-photon processes. We further investigate the dependence of the intensity-saturated graphene conductivity on doping, temperature, and optical frequency. Interestingly, we find a remarkably low intensity threshold for SA, which is consistent with available experimental reports [10–18]. Our calculations indicate a strong quenching of absorption depth produced by electrical doping (which can be controlled through gating), as well as a weak dependence on electron temperature. Additionally, through time-domain simulations based on an atomistic tight-binding/single-particle density-matrix formalism [40], we study SA in graphene nanoribbons, including finite-size effects and electron-electron interactions that play a significant role in the optical response of nanostructured graphene. Surprisingly, we find that while the linear absorption predicted in atomistic simulations is reduced compared to that of extended graphene, its nonlinear saturation intensity threshold is in good quantitative agreement with predictions based on the MDF model. Deviations from the semianalytical treatment occur only at high doping, where SA is quenched and multiphoton processes lead to an intensity-dependent increase of absorption. We anticipate that the present findings will impact the future development of graphene-based PML fibre lasers and single-mode random lasers.

## II. THEORETICAL MODEL

We consider a monochromatic optical field $\mathbf{E}(t) = \mathbf{E}_0 e^{-i\omega t} + \text{c.c.}$ of angular frequency $\omega$ and complex amplitude $\mathbf{E}_0$ impinging at normal incidence on a self-standing extended graphene sheet [see Fig. 1(a)]. At visible and lower frequencies, electrons in this material behave as MDFs, with their temporal evolution governed by the single-particle Dirac equation [41]

$$i\hbar\partial_t \psi_{\mathbf{k}}(t) = v_F \boldsymbol{\pi}\cdot\boldsymbol{\sigma}\psi_{\mathbf{k}}(t), \tag{1}$$

where $\hbar\mathbf{k}$ is the electron momentum, $\partial_t$ is the time derivative, $v_F \simeq c/300$ is the Fermi velocity, $c$ is the speed of light in vacuum, $\hbar$ is the reduced Planck constant, $\boldsymbol{\sigma} = (\sigma_x, \sigma_y)$ is the two-dimensional (2D) Pauli-matrix vector, and $\psi_{\mathbf{k}}(t)$ is the $\mathbf{k}$- and time-dependent two-component spinor accounting for the quantum states in the upper and lower Dirac-cone bands. The graphene band structure thus consists of two infinite cones, neglecting higher-band effects that are only relevant at high photon energies, above ~2 eV. We introduce an electron quasimomentum $\boldsymbol{\pi}$ that coincides with the unperturbed momentum (i.e., $\boldsymbol{\pi} = \hbar\mathbf{k}$) in the absence of external illumination. In this case, Eq. (1) admits spinor eigenvectors

$$\psi^{\pm}_{\mathbf{k},0}(t) = \frac{1}{\sqrt{2}}\begin{pmatrix} e^{-i\phi/2} \\ \pm e^{i\phi/2}\end{pmatrix} e^{-i\varepsilon_\pm t},$$

where $\varepsilon_\pm = \pm v_F k$ is the unperturbed conical dispersion of upper (+) and lower (−) energy bands [see Fig. 1(b)], while $\phi$ identifies the momentum direction, such that $\mathbf{k} = k(\cos\phi, \sin\phi)$, and a spatial dependence $e^{i\mathbf{k}\cdot\mathbf{r}}/\sqrt{\mathcal{A}}$ (normalized to the sheet area $\mathcal{A}$) is understood in the spinor.

In the presence of the impinging optical field, we use the customary minimal electron-light coupling prescription to write the electron quasimomentum as $\boldsymbol{\pi}(t) = \hbar\mathbf{k} + (e/c)\mathbf{A}(t)$, where $-e$ is the electron charge and $\mathbf{A}(t) = -c\int \mathbf{E}(t)dt$ is the potential vector in the Coulomb gauge ($\nabla\cdot\mathbf{A} = 0$). Without loss of generality, we assume the external light to be linearly polarized along the in-plane $x$ direction, so that $\mathbf{E}(t) = E_0 e^{-i\omega t}\hat{\mathbf{x}} + \text{c.c.}$ and $\mathbf{A}(t) = (cE_0/i\omega)e^{-i\omega t}\hat{\mathbf{x}} + \text{c.c.}$ Therefore, the incident field induces an oscillatory shift of the unperturbed bands $\varepsilon_\pm$ along $k_x$ around $\mathbf{k} = 0$ [see Fig. 1(b)]. Following the nonperturbative approach developed by Ishikawa [42,43], which we review in this section for the sake of completeness, we write the time-dependent spinor as a linear combination of the instantaneous upper- and lower-cone states

$$\psi_{\mathbf{k}}(t) = c^+_{\mathbf{k}}(t)\psi^+_{\mathbf{k}}(t) + c^-_{\mathbf{k}}(t)\psi^-_{\mathbf{k}}(t), \tag{2}$$

where

$$\psi^{\pm}_{\mathbf{k}}(t) = \frac{1}{\sqrt{2}}\begin{pmatrix} e^{-i\theta_{\mathbf{k}}(t)/2} \\ \pm e^{i\theta_{\mathbf{k}}(t)/2}\end{pmatrix} e^{\mp i\Omega_{\mathbf{k}}(t)}, \tag{3}$$

$\Omega_{\mathbf{k}}(t) = v_F\int|\mathbf{k} + (e/\hbar c)\mathbf{A}(t)|dt$ is a global dynamical phase, and $\theta_{\mathbf{k}}(t) = \text{atan}\{k_y/[k_x + (e/\hbar c)A(t)]\}$ is the time-dependent direction angle of the electron quasimomentum $\boldsymbol{\pi}$. We now insert the ansatz provided by Eq. (2) into Eq. (1) and define the interband coherence $\rho_{\mathbf{k}} = c^+_{\mathbf{k}}c^{-*}_{\mathbf{k}}$ and the population difference $n_{\mathbf{k}} = |c^+_{\mathbf{k}}|^2 - |c^-_{\mathbf{k}}|^2$. Without making any approximations, we can then rewrite the two-dimensional Dirac equation for MDFs in the form of generalized Bloch equations (GBEs) [42,43],

$$\dot{\rho}_{\mathbf{k}}(t) = -\frac{i}{2}\dot{\theta}_{\mathbf{k}}(t)n_{\mathbf{k}}(t)e^{2i\Omega_{\mathbf{k}}(t)}, \tag{4a}$$

$$\dot{n}_{\mathbf{k}}(t) = 2\dot{\theta}_{\mathbf{k}}(t)\text{Im}\{\rho_{\mathbf{k}}(t)e^{-2i\Omega_{\mathbf{k}}(t)}\}. \tag{4b}$$

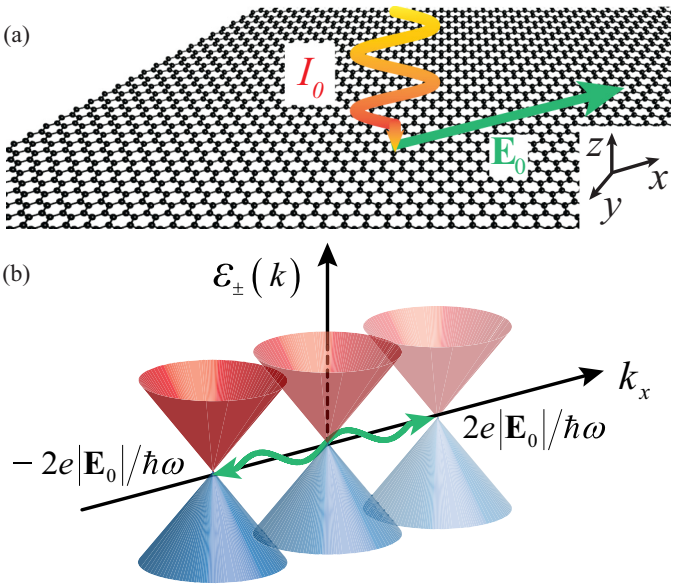


FIG. 1. (a) Schematic representation of a light wave (angular frequency $\omega$, amplitude $\mathbf{E}_0$, and intensity $I_0$) normally impinging on a self-standing graphene sheet. (b) Illustration of the temporal displacement of the Dirac cone along the $k_x$ direction due to the oscillatory optical field. The central cone represents the unperturbed conical dispersion of graphene ($\varepsilon_\pm$), while left and right cones indicate the maximum achievable displacement.

Then, the temporal evolution of graphene electrons can be evaluated by solving the above equations in the time domain and setting the initial conditions $\rho_{\mathbf{k}}(-\infty)=0$ and $n_{\mathbf{k}}(-\infty)=\mathcal{N}(k)=\mathcal{F}(k)-\mathcal{F}(-k)$, where $\mathcal{F}(k)=1/\{1+\exp[(v_{\mathrm{F}}\hbar k-\mu)/k_{\mathrm{B}}T]\}$ is the Fermi-Dirac occupation number, $\mu$ is the chemical potential, $k_{\mathrm{B}}$ is the Boltzmann constant, and $T$ is the electron temperature. Although we base our analysis on CW illumination conditions, we argue that these results are also applicable to commonly-used optical pulses that have a large duration compared with the optical period. Consequently, the derivations provided below, which are obtained for constant light intensity $I_0$, are equally valid for a situation in which the externally applied intensity $I_0(t)$ varies slowly over time, in the so-called slowly-varying-envelope approximation (SVEA). In other words, we assume that electron motion occurring over the fast temporal scale of the optical period adiabatically follows the slowly-varying temporal intensity profile in a quasi-steady-state. The single-electron current is thus obtained as

$$\begin{aligned}\mathbf{j}_{\mathbf{k}}(t)&=(-e/\hbar)\langle\psi_{\mathbf{k}}(t)|\nabla_{\mathbf{k}}[v_{\mathrm{F}}\boldsymbol{\pi}\cdot\boldsymbol{\sigma}]|\psi_{\mathbf{k}}(t)\rangle\\&=-ev_{\mathrm{F}}\big[n_{\mathbf{k}}\cos\theta_{\mathbf{k}}-2\sin\theta_{\mathbf{k}}\mathrm{Im}\big\{\rho_{\mathbf{k}}\mathrm{e}^{-2i\Omega_{\mathbf{k}}}\big\}\big]\hat{\mathbf{x}}\\&\quad-ev_{\mathrm{F}}\big[n_{\mathbf{k}}\sin\theta_{\mathbf{k}}+2\cos\theta_{\mathbf{k}}\mathrm{Im}\big\{\rho_{\mathbf{k}}\mathrm{e}^{-2i\Omega_{\mathbf{k}}}\big\}\big]\hat{\mathbf{y}}.\end{aligned}\tag{5}$$

We emphasize that this expression for the microscopic current is obtained without making any approximation beyond the MDF picture. The $n_{\mathbf{k}}$ terms account for the intraband current, while the remaining terms, which depend on the coherence $\rho_{\mathbf{k}}$, arise from interband dynamics [42,43]. One should note that the intraband current of the valence band $n_{\mathbf{k}}\cos\theta_{\mathbf{k}}$ should vanish when it is fully filled ($n_{\mathbf{k}}=-1$) in virtue of a well-known sum rule (see Ref. [44]). The macroscopic induced surface current $\mathbf{J}(t)$ is finally obtained by integrating over all electron momenta,

$$\mathbf{J}(t)=\frac{g_{\mathrm{s}}g_{\mathrm{v}}}{(2\pi)^2}\int\mathbf{j}_{\mathbf{k}}(t)d^2\mathbf{k},\tag{6}$$

where $g_{\mathrm{s}}=g_{\mathrm{v}}=2$ accounts for spin and valley degeneracies, and the integral extends over the entire 2D $\mathbf{k}$ plane. It is important to note that this integral is ill behaved due to the unphysical assumption of an infinitely extended valence band (i.e., for arbitrarily large $k$'s). The noted sum rule explains that this divergence must disappear in real systems due to the periodicity of the band in $\mathbf{k}$ space. We present an alternative regularization procedure to tackle this problem in the Supplemental Material (SI) [45], from which we conclude that the $n_{\mathbf{k}}$ factors in Eq. (5) must be replaced by $n_{\mathbf{k}}+1$ when calculating the integral of Eq. (6), and this prevents the divergence since $n_{\mathbf{k}}\to-1$ for large $k$'s. We also remark that, although the carrier current $\mathbf{j}_{\mathbf{k}}$ has both $\hat{\mathbf{x}}$ and $\hat{\mathbf{y}}$ components, the integrated macroscopic current remains polarized along $\hat{\mathbf{x}}$ and thus parallel to the external field. This theoretical framework describes the optical response of graphene in a single-electron picture, but it still neglects inelastic electron transitions that are produced for example by impurity scattering and coupling to phonons. In the following sections, these interactions are introduced phenomenologically through an effective electron lifetime. Additionally, we argue that the response of graphene, quantified as a 2.3% absorption at low intensities, is sufficiently weak as to ignore Coulomb self-interaction among induced charges [46,47]. As shown in the following sections, the theoretical framework provided here, and first developed by Ishikawa [42,43], reproduces the seminal predictions by Mikhailov [27–29] based on a nonperturbative description of intraband electron dynamics and those based on the well-established semiconductor Bloch equations (SBEs) [48]. Indeed, graphene SBEs constitute a particular limit that is valid when the temporally oscillating displacement of Dirac cones due to the sinusoidal optical momentum (pictorially illustrated in Fig. 1) is neglected (see below).

## III. INTRABAND SATURABLE ABSORPTION

We focus first on the purely intraband contribution to saturable absorption, i.e., neglecting interband dynamics. This contribution to SA, dependent only on the thermal distribution of conduction electrons, dominates in doped graphene for photon energies smaller than twice the Fermi level (i.e., $\hbar\omega<2E_{\mathrm{F}}$), for which one-photon interband transitions are prohibited by the Pauli exclusion principle; however, in this regime, two-photon absorption can overpower the SA effect, as we show later in Sec. V.

To describe the purely intraband response, one need not solve explicitly the GBEs, as it is sufficient to set $\rho_{\mathbf{k}}=0$ and $n_{\mathbf{k}}=\mathcal{N}(k)+1$, resulting in the macroscopic current

$$\mathbf{J}_{\mathrm{intra}}(t)=-\frac{ev_{\mathrm{F}}}{\pi^2}\hat{\mathbf{x}}\int[\mathcal{N}(k)+1]\cos\theta_{\mathbf{k}}(t)d^2\mathbf{k}.\tag{7}$$

We remark that, without a subtle but relevant modification of the potential vector, absorption is not described by this nonperturbative expression, which leads to the well-known lossless intraband current obtained by means of the Boltzmann transport equation [27–29]. We note that the mathematical procedure developed here is inspired by such seminal works, with the further inclusion of inelastic electron collisions in a nonperturbative manner. A phenomenological treatment of this effect requires a modification of the minimal coupling substitution, which ensues from the assumption that electrons are freely driven by the external electric field. Thus, we modify heuristically the definition of the direction angle $\theta_{\mathbf{k}}(t)$, assuming that the electron quasimomentum satisfies

$$\dot{\boldsymbol{\pi}}+\tau^{-1}(\boldsymbol{\pi}-\hbar\mathbf{k})=-e\mathbf{E}(t),\tag{8}$$

where $\tau$ is the characteristic inelastic collision time. We assume a value $\tau=22$ fs throughout this work, which is consistent with recent experiments [49–52]. We find Eq. (8) to admit the straightforward analytical solution $\boldsymbol{\pi}(t)=\hbar\mathbf{k}+(e/c)\mathbf{a}(t)$, where

$$\mathbf{a}(t)=-c\mathrm{e}^{-t/\tau}\int_{-\infty}^{t}\mathbf{E}(t')\mathrm{e}^{t'/\tau}dt'=\frac{cE_0\mathrm{e}^{-i\omega t}}{i\omega-1/\tau}\hat{\mathbf{x}}+\mathrm{c.c.}.\tag{9}$$

This modified expression effectively accounts for intraband electron collisions, and in particular, the direction angle of the electron momentum now becomes $\theta_{\mathbf{k}}(t)=\arctan\{k_y/[k_x+(e/\hbar c)a(t)]\}$. Incidentally, the $\tau\to\infty$ limit of $\boldsymbol{\pi}(t)$ reduces to the expression $\hbar\mathbf{k}+(e/c)\mathbf{A}(t)$ that was used in Sec. II.

In the limit of vanishing temperature ($T\to0$) the chemical potential coincides with the Fermi energy $\mu=E_{\mathrm{F}}$, the population inversion distribution becomes $\mathcal{N}(\mathbf{k})\to-\Theta(k-k_{\mathrm{F}})$,

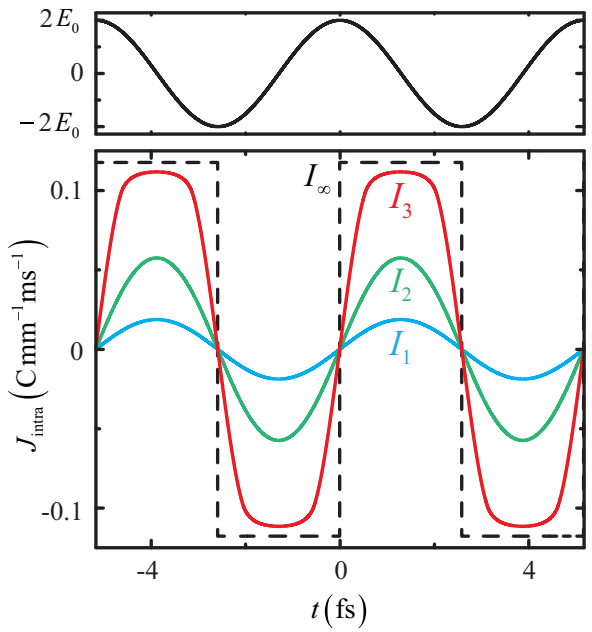


FIG. 2. Intraband surface current density $J_{\rm intra}(t)$ (lower panel) induced in extended graphene by a harmonic external electric field (upper panel) with maximum amplitude $2E_0 = \sqrt{8\pi I_0/c}$ and optical frequency $\omega = 2\pi c/\lambda$, where $\lambda = 1550$ nm is the optical excitation wavelength. In the lower panel we provide results for incident intensities $I_0 = 10$, 100, and 1000GW/cm$^2$, compared with the maximum achievable current density $J_{\rm max}(t)$ in the $I_0 \to \infty$ limit (dashed curve). We assume a high Fermi energy $E_{\rm F} = 1$ eV and zero temperature in order to illustrate the intraband contribution to the current when it is dominant over the interband one ($2E_{\rm F}/\hbar\omega = 2.5$).

where $\Theta$ is the Heaviside step function, and the integral in Eq. (7) can be solved analytically:

$$\mathbf{J}_{\rm intra}(t) = \hat{\mathbf{x}}\frac{-2eE_{\rm F}^2}{\pi^2\hbar^2 v_{\rm F}}\sqrt{1+[(e/\hbar c)a(t)/k_{\rm F}]^2} \times\int_0^{\pi/2}\cos\phi[\sqrt{1+f(t)\cos\phi}-\sqrt{1-f(t)\cos\phi}]d\phi, \tag{10}$$

where $k_{\rm F} = E_{\rm F}/\hbar v_{\rm F}$ is the Fermi wave number, $f(t) = 2(e/\hbar c)a(t)k_{\rm F}/\{k_{\rm F}^2 + [ea(t)/\hbar c]^2\}$, and the integral over $\phi$ can be expressed in terms of generalized Jacobi elliptic functions (see Refs. [53,54] and SI [45]). We emphasize that the intraband surface current density in Eq. (10) is highly nonlinear when $|E_0| > E_{\rm S}$, where $E_{\rm S} = \hbar\omega k_{\rm F}/e$ is the intraband saturation field. Additionally, the series expansion of Eq. (10) in powers of the electric field amplitude $E_0$,

$$\mathbf{J}_{\rm intra}(t) \simeq \frac{e^2}{\pi\hbar^2}{\rm Re}\left\{\frac{2iE_{\rm F}E_0 e^{-i\omega t}}{\omega+i\tau^{-1}} + \frac{ie^2v_{\rm F}^2E_0^3e^{-3i\omega t}}{4E_{\rm F}(\omega+i\tau^{-1})^3} - \frac{3ie^2v_{\rm F}^2|E_0|^2E_0e^{-i\omega t}}{4E_{\rm F}(\omega-i\tau^{-1})(\omega+i\tau^{-1})^2}\right\}\hat{\mathbf{x}} + \mathcal{O}(E_0^5), \tag{11}$$

fully reproduces the result obtained by means of the Boltzmann transport equation in the relaxation-free limit $\tau \to \infty$ [27–29]. In order to illustrate intraband saturable absorption of extended graphene, we plot in Fig. 2 the intraband current density calculated from Eq. (10) for several values of the incident light intensity $I_0 = (c/2\pi)|E_0|^2$. Note that, although the Fermi level $E_{\rm F} = 1$ eV used in the plot is high, comparable values have been achieved experimentally through top gating [55] and chemical doping [56]. Notice also that, when $I_0 \sim I_{\rm S}^{\rm intra}$, where $I_{\rm S}^{\rm intra} = (c/8\pi)|E_{\rm S}|^2$ is the saturation intensity (e.g., $I_{\rm S}^{\rm intra} \simeq 196$ GW/cm$^2$ at $\lambda = 1550$ nm), the current density also saturates, acquiring a square-like-wave temporal profile, as originally demonstrated by Mikhailov [27–29]. This can be verified analytically upon examination of the $E_0 \to \infty$ limit of Eq. (10), which yields the maximum achievable surface current density in doped graphene,

$$\mathbf{J}_{\rm max}(t) = -eNv_{\rm F}{\rm sign}[a(t)]\hat{\mathbf{x}}, \tag{12}$$

where $N = k_{\rm F}^2/\pi$ is the density of doping electrons. Then, as a consequence of current saturation, intraband absorption also saturates. We describe this effect quantitatively by defining an intraband absorption coefficient as the ratio of the time average of the absorbed power, which is simply evaluated over a single optical cycle, to the incident-light intensity,

$$\alpha_{\rm intra} \equiv \frac{\int_{-\pi/\omega}^{+\pi/\omega}\mathbf{J}_{\rm intra}(t)\cdot\mathbf{E}(t)dt}{(2\pi/\omega)I_0}. \tag{13}$$

This quantity reaches its maximum value $\alpha_{\rm max} = 4E_{\rm F}/[137\hbar\tau(\omega^2+\tau^{-2})]$ at low intensities and zero temperature. In contrast, it vanishes as $\alpha_{\rm intra} \simeq 1/\sqrt{I_0}$ in the limit of large incident intensity $I_0$. We further examine the $I_0$ dependence of $\alpha_{\rm intra}(I_0)$ for several Fermi energies [Fig. 3(a)] and electron temperatures [Fig. 3(b)] by numerically solving Eqs. (7) and (13). A strong dependence on Fermi energy is observed, as well as large thermal modulation at high electron temperatures exceeding $T \sim 5000$ K. We find that the depth of thermal modulation in the intraband absorption is roughly proportional to the Fermi energy and vanishes in undoped graphene. Typical intensities at which the intraband absorption saturates are of the order of 100–1000GW/cm$^2$, depending on the doping level. Note that the intraband saturation intensity $I_{\rm S}^{\rm intra}$ scales as the inverse square of the optical wavelength ($I_{\rm S}^{\rm intra} \propto \lambda^{-2}$), thus changing by a few orders of magnitude within the optical and near-infrared spectrum.

## IV. INTERBAND SATURABLE ABSORPTION

We now turn our attention to the effect of interband transitions on saturable absorption, neglecting purely intraband dynamics of thermalized electrons in the conduction band. This contribution becomes dominant for photon energies $\hbar\omega > 2E_{\rm F}$ (see below) and includes effects due to direct interband excitation as well as from intraband transitions enabled by the nonthermal electrons driven out-of-equilibrium. Interestingly, while the optical momentum $e\mathbf{A}(t)$ was found in Sec. III to produce sizable corrections to the intraband dynamics of thermal electrons in the conduction band, it does not affect interband dynamics significantly near its resonant contribution at $k = \omega/(2v_{\rm F})$, where the optical momentum is negligible [i.e., $\hbar k \gg (e/c)A(t)$]. Such an approximation is valid in the regime where the optical intensity remains low enough not to temporally displace the Dirac cone (see Fig. 1) up to the resonant electron wave number $k = \omega/(2v_{\rm F})$, leading to the

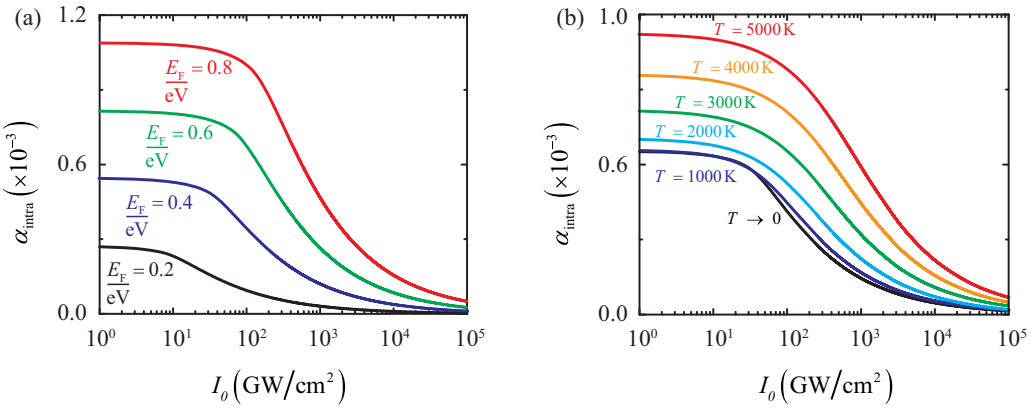


FIG. 3. Intraband absorption coefficient $\alpha_{\text{intra}}$ as a function of incident light intensity $I_0$ for (a) several Fermi energies ($E_F/\hbar\omega = 0.25, 0.5, 0.75, 1$) at zero temperature and (b) several electron temperatures ($k_B T/\mu = 0.22, 0.43, 0.65, 0.86, 1.08$) and fixed chemical potential $\mu = 0.4$ eV. The light wavelength is 1550 nm.

(safely met) condition $I_0 \ll 137\hbar\pi^3 c^4/2v_F^2\lambda^4 \approx 0.1$ TW/cm$^2$ at $\lambda = 1.55$ $\mu$m.

We consequently neglect $A(t)$, so that Eqs. (4) reduce to

$$\dot{\Gamma}_{\mathbf{k}} = -\left(\frac{1}{\tau} + 2i\omega_0\right)\Gamma_{\mathbf{k}} - \frac{ie}{\hbar k}\text{Re}\left\{E_0 e^{-i\omega t}\right\}\sin\phi\; n_{\mathbf{k}}, \quad (14a)$$

$$\dot{n}_{\mathbf{k}} = -\frac{1}{\tau}[n_{\mathbf{k}} - \mathcal{N}] + \frac{4e}{\hbar k}\text{Re}\left\{E_0 e^{-i\omega t}\right\}\sin\phi\; \text{Im}\{\Gamma_{\mathbf{k}}\}, \quad (14b)$$

where $\Gamma_{\mathbf{k}}(t) = \rho_{\mathbf{k}}(t)e^{-2i\omega_0 t}$, $\omega_0 = v_F k$, and we have introduced a phenomenological relaxation time $\tau$ that encompasses the effect of numerous ultrafast decay channels for out-of-equilibrium electrons into hot carriers and phonons [49–52]. We assume for simplicity a single effective relaxation time $\tau$, even though polarization dephasing and electron-hole recombination can take place over different timescales and their actual temporal dependences remain uncertain. Additionally, we use the same symbol $\tau$ for this quantity as in the intraband contribution (Sec. III), although we remark that the relative importance of different channels can differ substantially in both cases. Incidentally, Eqs. (14) coincide with the traditional Bloch equations for graphene and other two-band systems [48,57], which are routinely used to describe saturable absorption and other two-band effects, such as for example self-induced transparency [58–60]. To describe interband saturable absorption, we adopt the steady-state ansatz

$$\Gamma_{\mathbf{k}}(t) = \Gamma_{\mathbf{k}}^{+} e^{i\omega t} + \Gamma_{\mathbf{k}}^{-} e^{-i\omega t},$$

$$n_{\mathbf{k}}(t) = n_{\mathbf{k}}^{(0)} + \text{Re}\left\{n_{\mathbf{k}}^{(2)} e^{-2i\omega t}\right\}.$$

Using these expressions and neglecting higher-harmonic terms, Eqs. (14) lead to

$$n_{\mathbf{k}}^{(0)} = \mathcal{N} + 4\xi\;\text{Im}\left\{\frac{1 - i\omega\tau}{1 - i\omega_+\tau}\Gamma_{\mathbf{k}}^{-}\right\}, \quad (15a)$$

$$n_{\mathbf{k}}^{(2)} = \frac{-4i\xi(1 - i\omega\tau)\Gamma_{\mathbf{k}}^{-}}{(1 - 2i\omega\tau)(1 - i\omega_+\tau)}, \quad (15b)$$

$$\Gamma_{\mathbf{k}}^{+} = -\frac{1 + i\omega_-\tau}{1 + i\omega_+\tau}\Gamma_{\mathbf{k}}^{-*}, \quad (15c)$$

$$\Gamma_{\mathbf{k}}^{-} = \frac{(-i\xi/2)}{1 - i\omega_-\tau}\left(n_{\mathbf{k}}^{(0)} + \frac{1}{2}n_{\mathbf{k}}^{(2)}\right), \quad (15d)$$

where $\xi = (e\tau E_0/\hbar k)\sin\phi$ and $\omega_\pm = \omega \pm 2\omega_0$. While an analytical solution to Eqs. (15) is readily obtained, we omit the resulting expressions here, which are rather involved and do not provide much physical insight (these expressions are provided in the SI [45]). We emphasize that, by neglecting higher-harmonic terms in the solution of the Bloch equations, we are disregarding multiphoton absorption, which has been experimentally confirmed to be negligibly small in undoped graphene [61]. However, as we show in the next section, multiphoton absorption comes into play when one-photon processes are inhibited by the Pauli exclusion principle for $\hbar\omega/2E_F < 1$. The above analytical solutions nonperturbatively account for all single-photon processes, thus avoiding unphysical divergences associated with the Dirac point singularity. In addition, we remark that the solution above is found without assuming the so-called *rotating-wave approximation*, where the antiresonant terms $\Gamma_{\mathbf{k}}^{+}$ and $n_{\mathbf{k}}^{(2)}$ are neglected: Actually, such an approximation also leads to unphysical inconsistencies and divergences arising from the infinitely-extended Dirac cone assumption. The interband current density $\mathbf{J}_{\text{inter}}(t)$ is then obtained from this solution and Eq. (6) through the expression

$$\mathbf{J}_{\text{inter}}(t) = -\frac{2ev_F}{\pi^2}\text{Re}\left\{ie^{-i\omega t}\int \sin\phi\left[\Gamma_{\mathbf{k}}^{-} - \Gamma_{\mathbf{k}}^{+*}\right]d^2\mathbf{k}\right\}\hat{\mathbf{x}}. \quad (16)$$

We finally solve the 2D integral in $\mathbf{k}$ space numerically. Because we neglect third-harmonic terms, $\Gamma_{\mathbf{k}}$ oscillates in time around zero with the same angular frequency $\omega$ as the external field, while $n_{\mathbf{k}}$ oscillates with angular frequency $2\omega$ around the steady-state out-of-equilibrium population difference $n_{\mathbf{k}}^{(0)}$. Consequently, our approach enables the explicit calculation of the out-of-equilibrium occupation distribution of optically induced free carriers $f_c(\mathbf{k}) = [\mathcal{F}(k) + \mathcal{F}(-k) + n_{\mathbf{k}}^{(0)}]/2$ [see Figs. 4(a) and 4(b), where we plot $f_c(\mathbf{k})$ for several chemical potentials $\mu$ at fixed incident light intensity $I_0 = 10$ GW/cm$^2$

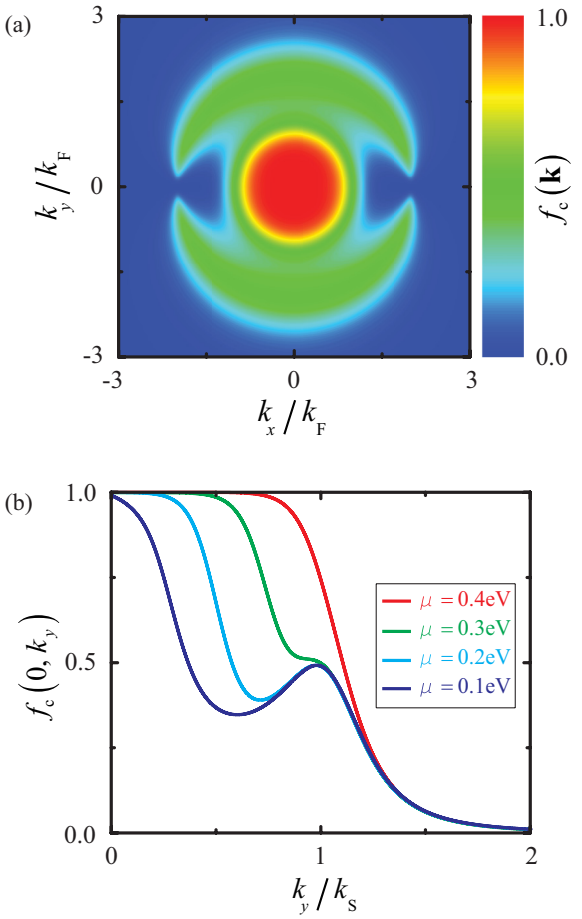


FIG. 4. (a) Out-of-equilibrium carrier occupation distribution $f_c(\mathbf{k})$ in 2D $\mathbf{k}$ space at $T = 300$ K for a chemical potential $\mu = 0.2$ eV ($\mu/\hbar\omega = 0.25$). The electron wave number components $k_x$ and $k_y$ are normalized to $k_F = \mu/\hbar v_F$. (b) Cut along the $k_y$ axis of (a) for several chemical potentials $\mu = 0.1$–$0.4$ eV ($\mu/\hbar\omega = 0.125,0.250,0.375,0.500$), with $k_y$ scaled to $k_S = \omega/2v_F$. The light intensity and wavelength are $I_0 = 10$ GW/cm$^2$ and $\lambda = 1550$ nm in both plots. We assume a phenomenological relaxation time $\tau = 22$ fs.

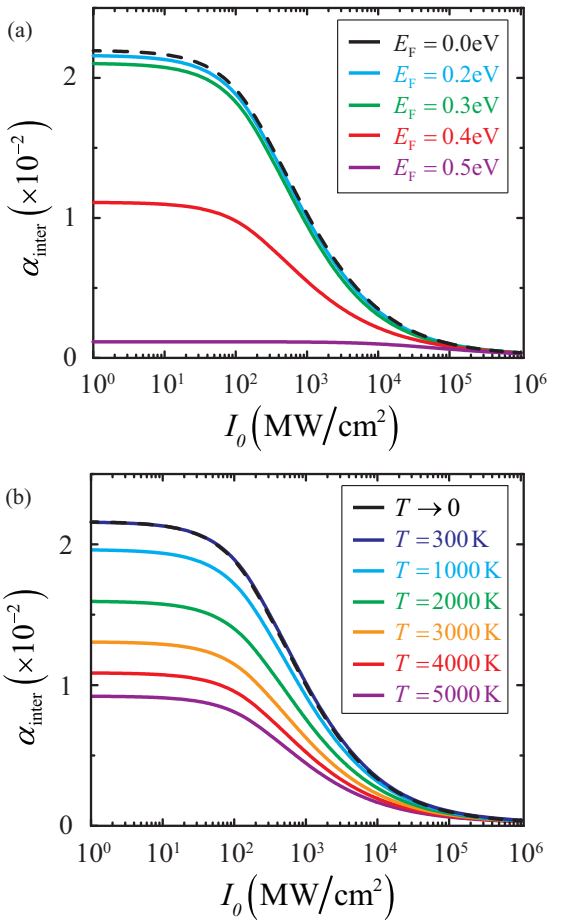


FIG. 5. Interband absorption coefficient $\alpha_{inter}$ as a function of incident light intensity $I_0$ for a wavelength of 1550 nm for (a) several Fermi energies ($E_F/\hbar\omega = 0,0.250,0.375,0.500,0.625$) at zero temperature and (b) several electron temperatures ($k_B T/\mu = 0.13,0.43,0.86,1.29,1.72,2.15$) and fixed chemical potential $\mu = 0.2$ eV. The inelastic relaxation time is set to $\tau = 22$ fs in all plots.

and wavelength $\lambda = 1550$ nm]. The $\mathbf{k}$-space steady-state carrier occupation $f_c(\mathbf{k})$ is characterized by two lobes along the $\hat{\mathbf{y}}$ axis, peaked at $(k_x,k_y) = (0,\pm\omega/2v_F)$ and surrounding the thermal Fermi-Dirac distribution of electrically doped thermal electrons [see Fig. 4(a)]. When $\hbar\omega < 2\mu$, the distribution $f_c(\mathbf{k})$ stays thermalized, as interband absorption is inhibited by the Pauli exclusion principle. In particular, after irradiation by an ultrashort optical pulse, $f_c(\mathbf{k})$ quickly evolves within a time of $\sim\tau = 22$ fs to a different thermal distribution corresponding to an increased electron temperature [57]. Eventually, it relaxes to the original unperturbed distribution $\mathcal{F}(k)$ within a timescale $\sim$ps due to electron-phonon scattering [49–51].

As a consequence of the optically induced out-of-equilibrium occupation $f_c(\mathbf{k})$ in the upper band, interband absorption also saturates. In simple terms, at high intensities the electron-hole recombinations produced by inelastic collisions balance the light-driven interband transitions, thus leading to absorption quenching. Similar to Sec. III, we attempt to quantitatively describe this effect by defining an interband absorption coefficient as the ratio of the time-averaged absorbed power over an optical cycle to the impinging intensity,

$$\alpha_{inter} \equiv \frac{\int_{-\pi/\omega}^{+\pi/\omega} \mathbf{J}_{inter}(t)\cdot\mathbf{E}(t)dt}{(2\pi/\omega)I_0}. \tag{17}$$

We calculate the intensity-dependent interband absorption coefficient $\alpha_{inter}(I_0)$ for several Fermi energies [Fig. 5(a)] and electron temperatures [Fig. 5(b)] by numerically solving Eqs. (16) and (17). For low intensities and zero temperature, we reproduce the universal absorption law of undoped graphene, $\alpha_{inter} \approx \pi\alpha$ [46,47], where $\alpha \approx 1/137$ is the fine-structure constant. This result reflects a dispersionless linear conductivity $\sigma_0 = e^2/4\hbar$. In contrast, the interband absorption vanishes as $\alpha_{inter} \simeq 1/\sqrt{I_0}$ in the limit of large incident intensities $I_0$. This high-intensity behavior is similar to intraband absorption (see Sec. III). We also observe a strong dependence of $\alpha_{inter}(I_0)$ on the Fermi energy, as well as a large thermal modulation at high electron temperatures $T \simeq 2000$ K. It should be noted that the modulation depth is much higher for interband than for intraband absorption, and additionally, it can be efficiently controlled by changing the Fermi energy.

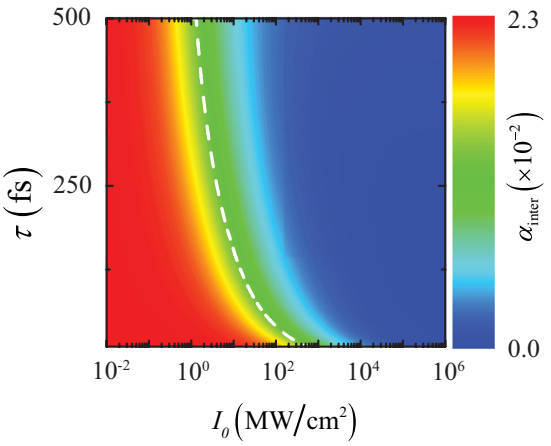


FIG. 6. Dependence of the interband absorption coefficient $\alpha_{\rm inter}$ of undoped graphene on incident light intensity $I_0$ and inelastic relaxation time $\tau$ at zero temperature. The white dashed curve represents the saturation intensity $I_{\rm S}^{\rm inter}(\tau)$ for which $\alpha_{\rm inter}(I_{\rm S}^{\rm inter}) = \alpha_{\rm inter}(0)/2$. The light wavelength is 1550 nm.

The light intensity required to achieve saturated absorption can be affected by the actual value of the inelastic collision time. For large $\tau$, optically pumped electrons are expected to produce Pauli blocking during a longer time, therefore reducing the interband saturation intensity $I_{\rm S}^{\rm inter}$. A plot of $\alpha_{\rm inter}$ as a function of $I_0$ and $\tau$ [Fig. 6(a), calculated for $\lambda = 1550$ nm] confirms this intuition and further reveals that $I_{\rm S}^{\rm inter}$ varies over a wide range (1–100 MW/cm$^2$) when $\tau$ evolves within a range compatible with reported measurements of the electron inelastic lifetime in graphene samples of different qualities. But more importantly, the actual values of $I_{\rm S}^{\rm inter}$ are much smaller than the characteristic intraband saturation intensities $I_{\rm S}^{\rm intra}$ derived in Sec. III. The interband saturation intensity $I_{\rm S}^{\rm inter}$ heavily depends on the optical wavelength $\lambda$ [see Fig. 7, where we plot $I_{\rm S}^{\rm inter}(\lambda)$ for several relaxation times $\tau$], varying by several orders of magnitude within the optical and near-infrared spectrum.

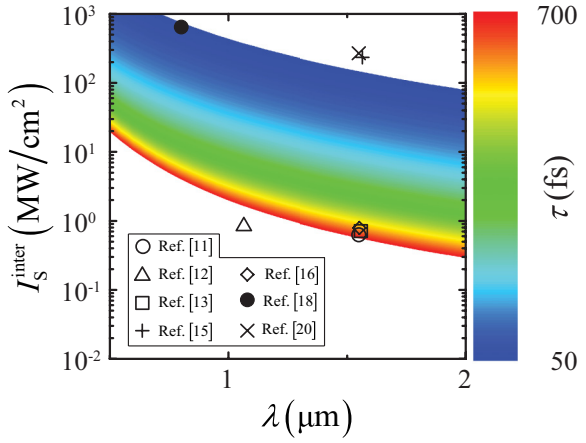


FIG. 7. Predicted interband saturation intensity $I_{\rm S}^{\rm inter}$ (left scale) as a function of optical wavelength $\lambda$ (horizontal axis) and relaxation time $\tau$ (color scale) at zero temperature and vanishing Fermi energy $E_{\rm F} = 0$. Available experimental results for the saturation intensity are indicated by symbols [10–18] (see legend).

We emphasize that the semianalytical framework developed above is highly accurate and computationally efficient, as the only numerical effort to be taken lies in the integration of the analytical expression for the microscopic current density over the reciprocal space [see Eq. (16)]. In this respect, we remark that the $\phi$ dependence of the integrand of Eq. (16) enters only through $\sin^2\phi$-like terms, and thus the integration over reciprocal space can be limited to the first quadrant (times a factor of 4). Consequently, in contrast to fully-numerical investigations [17,37,38], our method produces highly accurate results with only a few seconds of CPU. Further, our nonperturbative semianalytical treatment facilitates the exploration of graphene electron dynamics and their out-of-equilibrium distribution. In principle, previously reported perturbative treatments [30–36] can also provide some limited insight into the order of magnitude of the saturable absorption threshold for finite doping (see SI [45], where we compare perturbative and nonperturbative results). In contrast, they become highly inaccurate at low doping as a result of the inherent singularity at the Dirac point. Once more, this confirms the highly nonperturbative character of graphene at relatively moderate illumination intensities.

## V. FINITE-SIZE AND ATOMISTIC EFFECTS

Although we have provided a comprehensive theory of saturable absorption in extended graphene, practical devices operating on this principle must be finite in size. In narrow graphene nanoribbons only a few tens of nanometers wide, discretization of the electronic bands due to lateral confinement opens energy gaps and substantially modifies the optical response [62]. We contrast next the above theoretical description for extended graphene with results obtained from an atomistic approach for finite structures. Specifically, following the methods of Refs. [40,63], we simulate the intensity-dependent optical response of one-dimensional graphene nanoribbons by numerically solving the single-particle density matrix equation of motion in the time domain, using a tight-binding Hamiltonian for the $\pi$-band electronic structure along with a self-consistent electron-electron (Hartree) interaction potential (see SI [45] for further details).

Remarkably, for a nanoribbon of only ~20 nm width, we find the atomistic simulations of the intensity-dependent absorbed power under cw illumination to be in excellent qualitative agreement with that for extended graphene based on the MDF picture (see Fig. 8, where we compare results from the two methods for several Fermi energies at an excitation wavelength of 1550 nm). Quantitative discrepancies in the predictions are due to electron-electron interactions, finite-size, and higher-band effects that are relevant in nanostructured graphene but inherently absent in the MDF picture. However, these phenomena are found to affect mainly the unsaturated absorption coefficients in the weak intensity limit, while the nonlinear saturation intensity threshold shows good quantitative agreement with MDF predictions for extended graphene for most doping levels considered. Interestingly, for a Fermi energy of 0.5 eV ($\hbar\omega/2E_{\rm F} < 1$), the atomistic approach predicts an intensity-dependent increase in absorption rather than saturation (see Fig. 8). This discrepancy originates in multiphoton absorption processes: Although one-photon

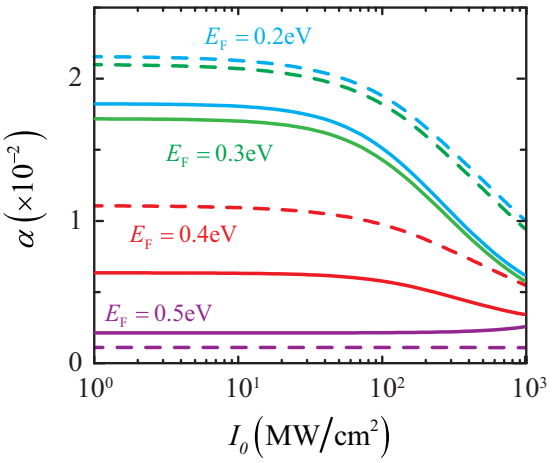


FIG. 8. Comparison between numerical atomistic simulations of a ribbon with zigzag edges and width $W = 20$ nm (solid curves) and the semianalytical MDF model for the total absorption coefficient ($\alpha = \alpha_{\mathrm{intra}} + \alpha_{\mathrm{inter}}$, dashed curves) as a function of incident light intensity $I_0$ for a wavelength of 1550 nm and several Fermi energies ($E_F/\hbar\omega = 0.250, 0.375, 0.500, 0.625$) in the vanishing temperature limit. In the atomistic calculations the incident light is polarized across the ribbon.

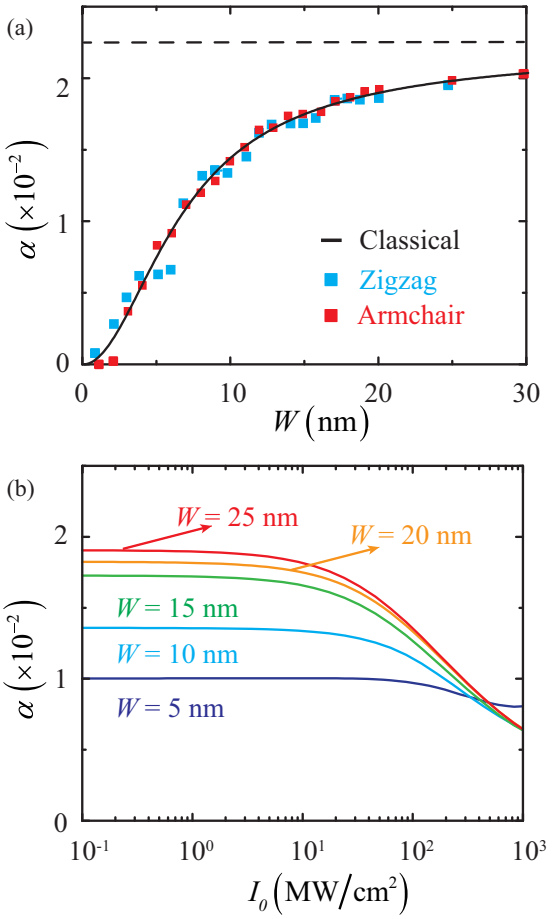


FIG. 9. Results from atomistic simulations of graphene ribbons depicting the dependence of the absorption coefficient $\alpha$ either (a) on ribbon width $W$ [for undoped graphene ($E_F = 0$) and both zigzag and armchair edges] and (b) on impinging light with intensity $I_0$ (polarized across the ribbon) for a fixed Fermi energy $E_F = 0.2$ eV and several values of $W$. The dashed line in (a) indicates the universal absorption limit $\alpha \approx \pi/137$.

absorption (for which the analytical derivation of the previous section is valid and accurate) is quenched at $\lambda = 1.55$ $\mu$m and $E_F = 0.5$ eV due to Pauli blocking, multiphoton absorption is not and leads to a small increase of absorption at very high intensities (as confirmed by perturbation theory estimates, see SI [45]). These results clearly indicate that the purely intraband contribution to SA does not play an important role because in the high doping case ($\hbar\omega/2E_F < 1$), where its modulation depth becomes comparable with the interband contribution, it is fully overpowered by multiphoton processes, leading to an intensity-dependent *increase* of absorption rather than quenching. These findings indicate that SA occurs only in the $\hbar\omega/2E_F > 1$ regime and that electrical doping quenches the modulation depth. A detailed description of multiphoton absorption goes beyond the scope of the present discussion but certainly warrants future investigation.

In Figure 9 we present atomistic simulations of the linear absorption coefficient $\alpha$ in graphene nanoribbons with either armchair- or zigzag-type edge terminations as a function of their width $W$, along with the nanoribbon absorption predicted by a classical electrodynamic description [full black curve in Fig. 9(a)]. Both levels of description predict an increase in absorption with nanoribbon width, eventually converging with the established 2.3% value of extended graphene. This result explains the offset in absorption observed in Fig. 8 when comparing atomistic and MDF results, which is reasonable given the reduced geometrical cross section in nanoribbons compared to extended graphene.

## VI. COMPARISON WITH EXPERIMENTS

We seek to compare our theoretical results with experimental data available in the literature. Most experimental studies exploit graphene as a saturable absorber for PML applications and thus focus on undoped or poorly doped samples, for which only interband absorption is relevant. Surprisingly, we find enormous variations in reported measurements, even for experiments conducted with the same light wavelength, so we attribute this dispersion in observed results to the different qualities of the graphene samples and experimental conditions (substrates, detectors, etc.). This intuition is supported by the calculations presented in Fig. 7 (see above), in which the saturation intensity for SA is shown to be highly dependent on the intrinsic relaxation time $\tau$, which is directly affected by the graphene sample quality. In contrast, the saturation intensity is less sensitive to doping (for $E_F < 2\hbar\omega$), although these parameters have a considerable effect on the modulation depth. In most photonic materials, SA is well described by a typical nonlinear absorption law $\alpha(I_0) = \alpha_0/[1 + I_0/I_S]$, for which $I_S$ is the saturation intensity such that $\alpha(I_0) = \alpha_0/2$, where $\alpha_0$ is the linear absorption coefficient. However, we find that the peculiar band structure of graphene produces a qualitatively different intensity dependence of the absorbance, which for both intraband and interband regimes is analytically found to follow a large-intensity asymptotic behavior $\alpha(I_0) \simeq 1/\sqrt{I_0/I_S}$ (see Secs. III and IV). As a result of this difference in asymptotic

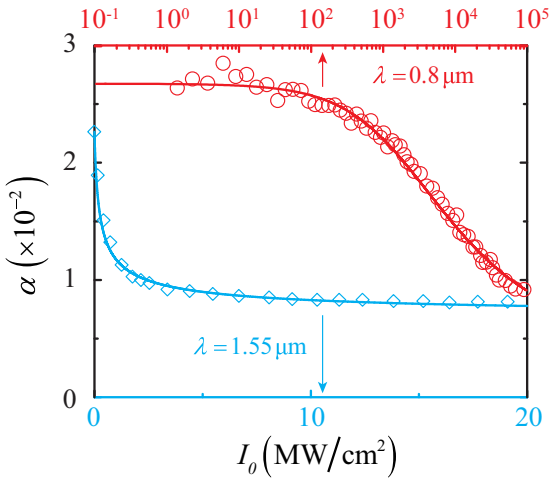


FIG. 10. Fitted analytical expression for the intensity-dependent absorption coefficient (curves) $\alpha(I_0) = \alpha_{ns} + \alpha_0/\sqrt{(1 + 3I_0/I_S)}$ of undoped graphene ($E_F = 0$) compared with experiments (symbols) at two different optical wavelengths: $\lambda = 800$ nm (red curves and symbols, $\alpha_{ns} = 0.008$) and $\lambda = 1550$ nm (blue curves and symbols, $\alpha_{ns} = 0.004$). Experimental results are taken from Refs. [11] (rhombic markers) and [18] (circle markers).

behavior, we argue that experimental data on graphene SA are much better fitted by the approximate expression $\alpha(I_0) = \alpha_0/\sqrt{(1 + 3I_0/I_S)}$. The high-intensity decay of absorption is thus slower than in common photonic materials, a result that matches well with available experimental data (see Fig. 10).

In Fig. 7 we compare the calculated saturation intensity (color plot) to experimental measurements (symbols) for several optical wavelengths and relaxation times. We find good agreement with several experimental results by assuming reasonable values for the relaxation times <100 fs reflecting the different sample qualities, while other experiments can only be reproduced with high relaxation times >500 fs [11–13,16]. We also note that a nonvanishing background absorption, which does not saturate within the considered range of illumination intensities, is usually present in the aforementioned experimental results [see Fig. 10, where we fit experimental data (symbols) with the predicted analytical expression for the intensity-dependent absorption coefficient (curves) $\alpha(I_0) = \alpha_{ns} + \alpha_0/\sqrt{(1 + 3I_0/I_S)}$, including an unsaturated background absorption term $\alpha_{ns}$]. This effect appears to be dependent on the number of graphene layers [11] and is found to vanish for pristine single-layer extended graphene [16].

## VII. CONCLUDING REMARKS

In summary, we have developed a nonperturbative and semianalytical description of both intraband and interband contributions to saturable absorption in extended graphene by modeling conduction electrons as 2D massless Dirac fermions coupled to an external optical field. The Dirac equation describing the time evolution of these electrons is recast in the form of generalized Bloch equations, which we solve semianalytically accounting only for one-photon processes. Remarkably, the interband contribution presents saturation at unusually low light intensities when compared with other materials, or with the intraband saturation. Additionally, we find a significant dependence of these effects on Fermi energy, providing an active mechanism of control over saturable absorption in the carbon layer via electrical doping modulation. Besides, when $\hbar\omega/2E_F < 1$, we find that multiphoton processes come into play and extended graphene does not behave as a saturable absorber. The electron temperature $T$ does not play a relevant role, unless $k_B T$ exceeds the Fermi energy or the incident photon energy. Nonetheless, $T$ can reach that regime under intense optical pumping, and therefore, this is an effect that must be considered when illuminating with long, intense light pulses.

We attribute the strong saturable absorption in graphene to its peculiar electronic band structure, and in particular, to the combination of its linear dispersion relation and the vanishing of the density of states at the Dirac point. Consequently, both doping and optical transitions in the presence of strong optical fields produce large modifications in the populations of electronic states, thus resulting in substantial variations in momentum and producing radical changes in the conductivity. We therefore expect a similarly low threshold for saturable absorption in other nanoscale materials that present Dirac cones or other exotic electronic structures characterized by a low density of electronic states at the Fermi level. Band-structure engineering is then a direction to explore in nanographenes, fullerenes, and carbon nanotubes, as well as in other van der Waals atomic-layer materials and its derivatives.

Interband absorption dominates under the conditions explored in currently available experiments, which are in good agreement with our analytical theory. In contrast, intraband saturation of absorption has not been observed in experiments due to the competing processes of multiphoton absorption. In this respect, our nonperturbative semianalytical predictions and atomistic calculations complement previous perturbative and fully numerical estimates and constitute a good reference for future experimental investigations. Indeed, the intraband saturation intensity scales as the inverse square of the optical wavelength and thus should become important at terahertz frequencies, particularly if it is enhanced by localized graphene plasmons in nanoislands/ribbons [64]. In this respect, while multiphoton processes can also be enhanced by localized plasmons [65], we anticipate that in general the nonlinear resonance shifts and the enhanced near fields in graphene nanostructures should contribute significantly to reduce the saturation intensity and enlarge the modulation depth of SA. A detailed study of plasmon-enhanced SA in graphene is still needed to explore how far the saturation intensity can be reduced. Overall, the extraordinarily low intensity threshold for saturable absorption in graphene, combined with its electrical tunability, offers great potential for photonic applications such as mode locking in graphene-clad fibre lasers and graphene-based random lasers.

## ACKNOWLEDGMENTS

This work has been partially supported by the Spanish MINECO (MAT2014-59096-P, Fundació Privada Cellex, and SEV2015-0522) and the European Commission (Graphene Flagship CNECT-ICT-604391 and FP7-ICT-2013-613024-GRASP).

[1] E. P. Ippen, Appl. Phys. B **58**, 159 (1994).
[2] R. Paschotta and U. Keller, Appl. Phys. B **73**, 653 (2001).
[3] G. Steinmeyer, D. H. Sutter, L. Gallmann, N. Matuschek, and U. Keller, Science **286**, 1507 (1999).
[4] N. Xiang, M. D. Guina, A. M. Vainionpaa, J. Lyytikainen, S. Suomalainen, M. J. Saarinen, O. Okhotnikov, T. Sajavaara, and J. Keinonen, IEEE J. Quantum Electron. **38**, 369 (2002).
[5] U. Keller, Nature (London) **424**, 831 (2003).
[6] A. G. Rozhin, Y. Sakakibara, S. Namiki, M. Tokumoto, and H. Kataura, Appl. Phys. Lett. **88**, 051118 (2006).
[7] V. Scardaci, Z. Sun, F. Wang, A. G. Rozhin, T. Hasan, F. Hennrich, I. H. White, W. I. Milne, and A. C. Ferrari, Adv. Mater. **20**, 4040 (2008).
[8] F. Wang, A. G. Rozhin, V. Scardaci, Z. Sun, F. Hennrich, I. H. White, W. I. Milne, and A. C. Ferrari, Nat. Nanotechnol. **3**, 738 (2008).
[9] Z. Sun, A. G. Rozhin, F. Wang, T. Hasan, D. Popa, W. O'Neill, and A. C. Ferrari, Appl. Phys. Lett. **95**, 253102 (2009).
[10] T. Hasan, Z. Sun, F. Wang, F. Bonaccorso, P. H. Tan, A. G. Rozhin, and A. C. Ferrari, Adv. Mater. **21**, 3874 (2009).
[11] Q. L. Bao, H. Zhang, Y. Wang, Z. H. Ni, Z. X. Shen, K. P. Loh, and D. Y. Tang, Adv. Funct. Mater. **19**, 3077 (2009).
[12] W. D. Tan, C. Y. Su, R. J. Knize, G. Q. Xie, L. J. Li, and D. Y. Tang, Appl. Phys. Lett. **96**, 031106 (2010).
[13] H. Zhang, D. Tang, R. J. Knize, L. Zhao, Q. Bao, and K. P. Loh, Appl. Phys. Lett. **96**, 111112 (2010).
[14] G. Xing, H. Guo, X. Zhang, T. C. Sum, and C. H. A. Huan, Opt. Express **18**, 4564 (2010).
[15] A. Martinez, K. Fuse, and S. Yamashita, Appl. Phys. Lett. **99**, 121107 (2011).
[16] Q. L. Bao, H. Zhang, Z. Ni, Y. Wang, L. Polavarapu, Z. Shen, Q.-H. Xu, D. Tang, and K. P. Loh, Nano Res. **4**, 297 (2011).
[17] T. Winzer, A. Knorr, M. Mittendorff, S. Winnerl, M.-B. Lien, D. Sun, T. B. Norris, M. Helm, and E. Malic, Appl. Phys. Lett. **101**, 221115 (2012).
[18] I. H. Baek, H. W. Lee, S. Bae, B. H. Hong, Y. H. Ahn, D.-I. Yeom, and F. Rotermund, Appl. Phys. Expr. **5**, 032701 (2012).
[19] G. Giovannetti, P. A. Khomyakov, G. Brocks, V. M. Karpan, J. van den Brink, and P. J. Kelly, Phys. Rev. Lett. **101**, 026803 (2008).
[20] Z. Sun, T. Hasan, F. Torrisi, D. Popa, G. Privitera, F. Wang, F. Bonaccorso, D. M. Basko, and A. C. Ferrari, ACS Nano **4**, 803 (2010).
[21] D. Popa, Z. Sun, F. Torrisi, T. Hasan, F. Wang, and A. C. Ferrari, Appl. Phys. Lett. **97**, 203106 (2010).
[22] Z. Sun, D. Popa, T. Hasan, F. Torrisi, F. Wang, E. J. R. Kelleher, J. C. Travers, V. Nicolosi, and A. C. Ferrari, Nano Res. **3**, 653 (2010).
[23] D. Popa, Z. Sun, T. Hasan, F. Torrisi, F. Wang, and A. C. Ferrari, Appl. Phys. Lett. **98**, 073106 (2011).
[24] H. Zhang, Q. Bao, D. Tang, L. Zhao, and K. Loh, Appl. Phys. Lett. **95**, 141103 (2009).
[25] H. Zhang, D. Y. Tang, L. M. Zhao, Q. L. Bao, K. P. Loh, B. Lin, and S. C. Tjin, Laser Phys. Lett. **7**, 591 (2010).
[26] A. Marini and F. J. García de Abajo, Phys. Rev. Lett. **116**, 217401 (2016).
[27] S. A. Mikhailov, Europhys. Lett. **79**, 27002 (2007).
[28] S. A. Mikhailov and K. Ziegler, J. Phys.: Condens. Matter **20**, 384204 (2008).
[29] S. A. Mikhailov, Physica E **40**, 2626 (2008).
[30] J. L. Cheng, N. Vermeulen, and J. E. Sipe, New J. Phys. **16**, 053014 (2014).
[31] N. M. R. Peres, Y. V. Bludov, J. E. Santos, A.-P. Jauho, and M. I. Vasilevskiy, Phys. Rev. B **90**, 125425 (2014).
[32] S. A. Mikhailov, Phys. Rev. B **90**, 241301(R) (2014).
[33] J. L. Cheng, N. Vermeulen, and J. E. Sipe, Phys. Rev. B **91**, 235320 (2015).
[34] J. L. Cheng, N. Vermeulen, and J. E. Sipe, New J. Phys. **18**, 029501 (2016).
[35] J. L. Cheng, N. Vermeulen, and J. E. Sipe, Phys. Rev. B **93**, 039904 (2016).
[36] S. A. Mikhailov, Phys. Rev. B **93**, 085403 (2016).
[37] Z. Zhang and P. L. Voss, Opt. Lett. **36**, 4569 (2011).
[38] J. L. Cheng, N. Vermeulen, and J. E. Sipe, Phys. Rev. B **92**, 235307 (2015).
[39] K. S. Novoselov, A. K. Geim, S. V. Morozov, D. Jiang, M. I. Katsnelson, I. V. Grigorieva, S. V. Dubonos, and A. A. Firsov, Nature (London) **438**, 197 (2005).
[40] J. D. Cox and F. J. García de Abajo, Nat. Commun. **5**, 5725 (2014).
[41] A. H. Castro Neto, F. Guinea, N. M. R. Peres, K. S. Novoselov, and A. K. Geim, Rev. Mod. Phys. **81**, 109 (2009).
[42] K. L. Ishikawa, Phys. Rev. B **82**, 201402(R) (2010).
[43] K. L. Ishikawa, New J. Phys. **15**, 055021 (2013).
[44] J. E. Sipe and E. Ghahramani, Phys. Rev. B **48**, 11705 (1993).
[45] See Supplemental Material at http://link.aps.org/supplemental/10.1103/PhysRevB.95.125408 for additional information on technical aspects of the theoretical methods used to model saturable absorption in infinitely-extended graphene and in graphene nanoribbons.
[46] R. R. Nair, P. Blake, A. N. Grigorenko, K. S. Novoselov, T. J. Booth, T. Stauber, N. M. R. Peres, and A. K. Geim, Science **320**, 1308 (2008).
[47] K. F. Mak, M. Y. Sfeir, Y. Wu, C. H. Lui, J. A. Misewich, and T. F. Heinz, Phys. Rev. Lett. **101**, 196405 (2008).
[48] H. Haug and S. W. Koch, *Quantum Theory of the Optical and Electronic Properties of Semiconductors*, 4th ed. (World Scientific, Singapore, 2004).
[49] J. C. Johannsen, S. Ulstrup, F. Cilento, A. Crepaldi, M. Zacchigna, C. Cacho, I. C. E. Turcu, E. Springate, F. Fromm, C. Raidel, T. Seyller, F. Parmigiani, M. Grioni, and P. Hofmann, Phys. Rev. Lett. **111**, 027403 (2013).
[50] I. Gierz, J. C. Petersen, M. Mitrano, C. Cacho, I. C. E. Turcu, E. Springate, A. Stöhr, A. Köhler, U. Starke, and A. Cavalleri, Nat. Mater. **12**, 1119 (2013).
[51] D. Brida, A. Tomadin, C. Manzoni, Y. J. Kim, A. Lombardo, S. Milana, R. R. Nair, K. S. Novoselov, A. C. Ferrari, G. Cerullo, and M. Polini, Nat. Commun. **4**, 1987 (2013).
[52] M. Trushin, A. Grupp, G. Soavi, A. Budweg, D. De Fazio, U. Sassi, A. Lombardo, A. C. Ferrari, W. Belzig, A. Leitenstorfer, and D. Brida, Phys. Rev. B **92**, 165429 (2015).
[53] M. Abramowitz and I. A. Stegun, *Handbook of Mathematical Functions* (Dover, New York, 1972).
[54] H. Dong, C. Conti, A. Marini, and F. Biancalana, J. Phys. B **46**, 155401 (2013).

[55] C. F. Chen, C. H. Park, B. W. Boudouris, J. Horng, B. Geng, C. Girit, A. Zettl, M. F. Crommie, R. A. Segalman, S. G. Louie, and F. Wang, Nature (London) **471**, 617 (2011).
[56] H. Liu, Y. Liu, and D. Zhua, J. Mater. Chem. **21**, 3335 (2011).
[57] E. Malic, T. Winzer, E. Bobkin, and A. Knorr, Phys. Rev. B **84**, 205406 (2011).
[58] S. L. McCall and E. L. Hahn, Phys. Rev. **183**, 457 (1969).
[59] H. Giessen, A. Knorr, S. Haas, S. W. Koch, S. Linden, J. Kuhl, M. Hetterich, M. Grün, and C. Klingshirn, Phys. Rev. Lett. **81**, 4260 (1998).
[60] A. Marini and F. Biancalana, Phys. Rev. Lett. **110**, 243901 (2013).
[61] H. Yang, X. Feng, Q. Wang, H. Huang, W. Chen, A. T. S. Wee, and W. Ji, Nano Lett. **11**, 2622 (2011).
[62] S. Thongrattanasiri, A. Manjavacas, and F. J. García de Abajo, ACS Nano **6**, 1766 (2012).
[63] J. D. Cox, I. Silveiro, and F. J. García de Abajo, ACS Nano **10**, 1995 (2016).
[64] M. M. Jadidi, J. C. König-Otto, S. Winnerl, A. B. Sushkov, H. D. Drew, T. E. Murphy, and Martin Mittendorf, Nano Lett. **16**, 2734 (2016).
[65] M. Jablan and D. E. Chang, Phys. Rev. Lett. **114**, 236801 (2015).